Development of a Numerical Phase Optimized Upwinding Combined Compact Difference Scheme for Solving the Camassa–Holm Equation with Different Initial Solitary Waves

C. H. Yu,[1,2] **Tony W. H. Sheu,**[2,3,4] **C. H. Chang,**[4] **S. J. Liao**[5]

[1] *Department of Ocean Science and Engineering, Zhejiang University, Yuhangtang Road, Hangzhou, Zhejiang, People's Republic of China*

[2] *Department of Engineering Science and Ocean Engineering, National Taiwan University, No. 1, Sec. 4, Roosevelt Road, Taipei, Taiwan, Republic of China*

[3] *Institute of Applied Mathematical Sciences, Department of Mathematics, National Taiwan University, Taipei, Taiwan, Republic of China*

[4] *Center of Advanced Study in Theoretical Sciences (CASTS), Department of Mathematics, National Taiwan University, Taipei, Taiwan, Republic of China*

[5] *School of Naval Architecture, Ocean and Civil Engineering, Shanghai Jiao Tong University, Shanghai, China*

Received 31 January 2013; accepted 6 January 2015
Published online in Wiley Online Library (wileyonlinelibrary.com).
DOI 10.1002/num.21965

In this article, the solution of Camassa–Holm (CH) equation is solved by the proposed two-step method. In the first step, the sixth-order spatially accurate upwinding combined compact difference scheme with minimized phase error is developed in a stencil of four points to approximate the first-order derivative term. For the purpose of retaining both of the long-term accurate Hamiltonian property and the geometric structure inherited in the CH equation, the time integrator used in this study should be able to conserve symplecticity. In the second step, the Helmholtz equation governing the pressure-like variable is approximated by the sixth-order accurate three-point centered compact difference scheme. Through the fundamental and numerical verification studies, the integrity of the proposed high-order scheme is demonstrated. Another aim of this study is to reveal the wave propagation nature for the investigated shallow water equation subject to different initial wave profiles, whose peaks take the smooth, peakon, and cuspon forms. The transport phenomena for the cases with/without inclusion of the linear first-order advection term κu_x in the CH equation will be addressed. Numer Methods Partial Differential Eq 000: 000–000, 2015

Keywords: Camassa–Holm equation; Hamiltonian; long-term accurate; upwinding combined compact difference scheme

Correspondence to: Tony W. H. Sheu, Department of Engineering Science and Ocean Engineering, National Taiwan University, No. 1, Sec. 4, Roosevelt Road, Taipei, Taiwan, Republic of China (e-mail: twhsheu@ntu.edu.tw)
Contract grant sponsor: National Science Council; contract grant number: NSC 99-2221-E-002-225-MY3
Contract grant sponsor: Fundamental Research Funds for the Central Universities; contract grant number: 2014QNA4030

I. INTRODUCTION

Unlike the integrable KdV and Boussinesq equations applied to study soliton wave interaction, the integrable Camassa–Holm (CH) equation given below can be used to model not only the soliton interaction but also the breaking of wave

$$u_t + 2\kappa u_x - u_{xxt} + 3uu_x = 2u_x u_{xx} + uu_{xxx}. \tag{1}$$

The solution of the nonlinear dispersive equation given above will be sought subject to the initial condition which satisfies $w(x,0) > 0$ and $\int_{\mathscr{R}} (1+|x|)^{1+l}(|w(x,0) - \kappa| + |w_x(x,0)| + |w_{xx}(x,0)|)dx < \infty$ for integers l. The momentum variable at $t = 0$ is $w(x,0) = u(x,0) - u_{xx}(x,0) + \kappa$ [1]. Equation (1) derived under the shallow water assumption has a positive constant $\kappa = (gh_0)^{1/2}$ in the inviscid limit, where g stands for the gravity and h_0 denotes the undisturbed water depth. Provided that $\kappa = 0$, Eq. (1) turns out to be the special case of the b-family of the equations $u_t - u_{xxt} + (b+1)uu_x = bu_x u_{xx} + uu_{xxx}$ [2]. This class of equations includes the integrable CH equation, where $b = 2$, and the Degasperis–Procesi equation, where $b = 3$ [3].

The CH equation has been the subject of intensive studies for many years for understanding its possible generation of breaking or peaked solitary wave, and other solitary waves whose natures are different at the peaks. Provided that there is a discontinuity in the first derivative at the solution peak, it is referred to as the peakon solution. In other words, peakon (or peaked solitary wave), by definition, is a soliton accommodating the finite-valued discontinuous first derivative term. As Eq. (1) permits peakon and cuspon solutions, calculation of these locally high gradient solutions near wave crest numerically is a challenging task.

In comparison with the first-order spatial derivative term and the temporal derivative term, both of the third-order spatial derivative term and the mixed space-time derivative term shown in Eq. (1) were much less studied numerically. For this reason, the third-order CH equation has been transformed to its equivalent system of equations containing only the first-order spatial and temporal derivative terms. In this spirit, the $u-m$ formulation was used in [4] to retain its symplectic solution property using the sixth-order accurate iterative symplectic Runge–Kutta scheme. All the first-order derivative terms were approximated by the proposed modified wavenumber optimized fourth-order accurate spatial scheme. This $u-m$ formulation failed to numerically resolve the peaked wave crest. The $u-P$ equations, which contain the equation $u_t + uu_x = -P_x$ and the inhomogeneous Helmholtz equation for P, were therefore applied to conserve not only the symplecticity but also preserve the numerical modified wavenumber. Moreover, application of the $u - P - \alpha$ formulation helps to capture peakon and cuspon sharp profiles. In this light, the energy density $\alpha = u^2 + u_x^2$ is taken into account in the simulation of CH equation by solving the transport equation $\alpha_t + (u\alpha)_x = -Q_x$ for α, where $Q = 2Pu - u^3 - 2\kappa u^2$ [6, 5].

In 1944, Camassa et al. showed that smooth solitary wave solutions are permitted for all $\kappa > 0$ but solutions with the derivative discontinuity are not allowed to appear at the peak of solitary wave [7]. In the stability analysis of the CH solitons, Constantin and Strauss [8] proved however that CH solution is stable under small disturbances. Similar to the finding in [9], Liao derived the peaked solitary wave for the case of $\kappa > 0$ through the Homotopic Analysis Method (HAM). However, such a peaked solitary wave has never been observed experimentally as $\kappa > 0$. This is the impetus for us to clarify numerically whether or not peaked solution is permitted in CH equation under the condition of $\kappa > 0$.

The rest of this article is organized as follows. The nonlinear CH equation and some of its intriguing solution natures will be presented in Section II. In Section III, the CH equation is transformed to a system of equations containing one equation for u with the reduced differential order

and the other inhomogeneous Helmholtz equation for P. In Sections IV.A—IV.C, the numerical methods developed for solving the equations shown in the $u-P$ formulation are described. Section IV.D is devoted to the dispersion analysis of the proposed combined compact difference scheme. In Section V, the CH solutions will be sought subject to different initial conditions for the CH equation with/without inclusion of the linear first-order advection term. Our objective is to show their traveling/nontraveling one-solitary wave natures. Finally, some concluding remarks will be drawn in Section VI.

II. CH EQUATION AND ITS DISTINGUISHED FEATURES

The nonlinear dispersive CH equation has many mathematically intriguing properties and physically rich phenomena. For example, CH equation has bi-Hamiltonian structure and has two associated infinite dimensional Hamiltonian formulations. This integrable equation possesses therefore infinitely many conservation laws. This mathematically fruitful wave equation accommodates many remarkable geometric structures. First, CH equation can be completely integrated through the Lax pair equations constructed by Camassa and Holm [10]. The CH equation is also classified to be multisymplectic. According to the work of Bridges and Reich [11], two variables $(\overline{\omega}, \overline{\kappa})$ exists which can conserve symplecticity because of $\frac{\partial \overline{\omega}}{\partial t} + \frac{\partial \overline{\kappa}}{\partial x} = 0$. Given an initial condition $u_0(x,\ t = 0)$ belonging to the Sobolev space H^1, Eq. (1) investigated at $\kappa = 0$, for example, has been shown to have the well-known conservation laws given in Section V [12–14].

III. ITERATIVE SOLUTION ALGORITHM

The dimensionless CH equation has two space-time mixed derivative and third-order dispersive terms. We are therefore motivated to rewrite Eq. (1) to the equivalent system of equations having only the first-order derivative terms. One can reduce the differential order of the CH equation by rewriting (1) to the equation $m_t + um_x + 2u_x m = -2\kappa u_x$, where the momentum variable is defined by $m = u - u_{xx} - \kappa$ [15, 16]. The CH equation can be also transformed to the $u - P$ system of equations. In the current study, the $u - P$ formulation is adopted as this formulation has been known to be more suitable to predict solitary wave propagation involving either a peakon or a cuspon.

Given a properly prescribed boundary condition, the solution u for (1) will be first sought subject to an initial condition $u(x, t = 0) = f \in H^1$ from the following nonlinear equation

$$u_t + uu_x = -P_x. \tag{2}$$

The variable P is known as the dimensionless pressure (or surface elevation) and is governed by

$$P - P_{xx} = u^2 + uu_x + 2\kappa u. \tag{3}$$

Thanks to Eqs. (2) and (3), Eq. (1) is classified to be elliptic-hyperbolic provided that the solution remains smooth.

IV. SYMPLECTIC SEMI-DISCRETIZATION METHOD

In the literature, Camassa and Lee [17–20] solved the Eq. (1), subject to different specified boundary conditions, by introducing a proper number of "particles" along the characteristic curve of CH

equation. In finite difference method, a rigorous convergence proof was presented in the work of Holden and Raynaud [21, 22]. The pseudospectral scheme of Kalisch and Lenells [23] has also been known to be applicable to predict the solution from the CH equation. The semidiscretized Fourier–Galerkin and Fourier-collocation methods were applied as well to get a convergent CH solution [24]. Peakon solutions were predicted by Artebrant and Schroll [25] using the adaptive upwinding finite volume discretization method. The local discontinuous Galerkin method has also been used to solve the CH equation [26]. Besides these numerical methods, the multisymplectic method [6], energy-conserving Galerkin method [27] and self-adaptive mesh method [28] have also been proposed previously to solve the currently investigated integrable equation. To get an accurately predicted result for the soliton-cuspon or the cuspon-cuspon problem, one can refer to [29] for additional details.

The CH Eq. (1) or Eqs. (2) and (3) can be recast in a symplectic or a multisymplectic formulation described in Section II. While solving this highly nonlinear equation, it is therefore essential to preserve its discrete invariance and local/global conservation laws using the methods underlying the geometric numerical integration. In this study the symplectic method [30, 31] is chosen. Symplectic numerical discretization refers to the approach of discretizing the integrable equation in space to a Hamiltonian ordinary differential equation (ODE). A symplectic method is then applied to preserve the discrete symplectic structure partly described in Section II. Within the context of the symplectic semidiscretization methods, approximation of the spatial and temporal derivative terms shown in (2) and (3) will be respectively given below.

A. Combined Compact Difference Scheme for u_x and P_x

To capture such a sharply varying solution near the peaks, we need to apply a scheme which can provide us a very accurate numerical phase at a smaller grid stencil. Otherwise, nonphysical oscillatory solution will appear. To get a well predicted CH solution, the scheme shall not only yield a higher accuracy in smooth region but can also capture the sharp solution. We are therefore motivated to develop an upwinding combined compact difference scheme with the smallest phase error in a grid of four-point stencil. The derivative terms $\frac{\partial u}{\partial x}$ and $\frac{\partial^2 u}{\partial x^2}$ are approximated implicitly as follows

$$a_1 \left.\frac{\partial u}{\partial x}\right|_{i-1} + \left.\frac{\partial u}{\partial x}\right|_{i} + a_3 \left.\frac{\partial u}{\partial x}\right|_{i+1} = \frac{1}{h}(c_1 u_{i-2} + c_2 u_{i-1} + c_3 u_i) - h\left(b_1 \left.\frac{\partial^2 u}{\partial x^2}\right|_{i-1} + b_2 \left.\frac{\partial^2 u}{\partial x^2}\right|_{i} + b_3 \left.\frac{\partial^2 u}{\partial x^2}\right|_{i+1}\right), \tag{4}$$

$$-\frac{1}{8}\left.\frac{\partial^2 u}{\partial x^2}\right|_{i-1} + \left.\frac{\partial^2 u}{\partial x^2}\right|_{i} - \frac{1}{8}\left.\frac{\partial^2 u}{\partial x^2}\right|_{i+1} = \frac{3}{h^2}(u_{i-1} - 2u_i + u_{i+1}) - \frac{9}{8h}\left(-\left.\frac{\partial u}{\partial x}\right|_{i-1} + \left.\frac{\partial u}{\partial x}\right|_{i+1}\right). \tag{5}$$

The derivative term $\frac{\partial^2 u}{\partial x^2}$ is approximated by the centered scheme. The coefficients shown in (5) can be derived simply by applying the method of Taylor series expansion to make the leading truncation error terms shown in the derived modified equations to be zero, yielding the sixth-order formal accuracy.

Derivation of the coefficients in (4) for the case involving a positive-valued convective coefficient is started by performing Taylor series expansion on the terms u_{i-2}, u_{i-1}, $\frac{\partial u}{\partial x}|_{i-1}$, $\frac{\partial u}{\partial x}|_{i}$, $\frac{\partial u}{\partial x}|_{i+1}$, $\frac{\partial^2 u}{\partial x^2}|_{i-1}$, $\frac{\partial^2 u}{\partial x^2}|_{i}$ and $\frac{\partial^2 u}{\partial x^2}|_{i+1}$ with respect to u_i. The modified equation for (4) is derived first and the seven leading truncation errors are then eliminated to get a set of

algebraic equations. One more algebraic equation is needed for uniquely determining all the eight introduced coefficients shown in (4) for $\frac{\partial u}{\partial x}|_i$.

Our strategy of reducing the dispersion error while approximating the first-order derivative term is to get a good match between the exact and numerical wavenumbers. One can refer to [32] for details about the exact wave number α and the numerical wave number α'. Note that the real and imaginary parts of the numerical modified wavenumber $\alpha' h$ are responsible respectively for the dispersion error (phase error) and the dissipation error (amplitude error). A better dispersive accuracy for α' can be obtained provided that the value of αh is closer to $\Re[\alpha' h]$, where $\Re[\alpha' h]$ denotes the real part of $\alpha' h$. The magnitude of the error function $E(\alpha)$ defined below should be very small and positive over the integration interval given below for αh

$$E(\alpha) = \int_0^{\frac{7\pi}{8}} [W \cdot (\alpha\, h - \Re[\alpha'\, h])]^2 d(\alpha h). \tag{6}$$

Employment of the weighting function W, which is chosen to be the denominator of $(\alpha\, h - \Re[\alpha'\, h])$ [33], enables us to analytically integrate $E(\alpha)$. To make the above error function to be positive and minimal, the extreme condition $\frac{\partial E}{\partial c_3} = 0$ is enforced to minimize the numerical wavenumber error. This constraint equation will be used together with the algebraic equations derived through the modified equation analysis to get not only a higher dissipation accuracy but also an improved dispersion accuracy. Note that $\frac{7\pi}{8}$ shown in (6) has been numerically determined so that we can get the smallest value of E.

The introduced unknown coefficients in (4) can now be uniquely determined as $a_1 = 0.888251$, $a_3 = 0.049229$, $b_1 = 0.150072$, $b_2 = -0.250712$, $b_3 = -0.012416$, $c_1 = 0.0166617$, $c_2 = -1.970804$ and $c_3 = 1.954143$. The above upwinding scheme developed for $\frac{\partial u}{\partial x}$ has the spatial accuracy of order six according to the following derived modified equation

$$\frac{\partial u}{\partial x} = \frac{\partial u}{\partial x}\bigg|_{exact} + 0.424003657 \times 10^{-6} h^6; \frac{\partial^7 u}{\partial x^7} + H.O.T.. \tag{7}$$

For $u < 0$, the proposed noncentered combined compact difference scheme can be similarly derived. The above sixth-order accurate upwinding combined compact difference scheme is also applied to approximate the gradient term P_x shown in (2).

B. Compact Difference Scheme for the Helmholtz Equation

The compact difference scheme originally developed in [4] for solving the variable Helmholtz equation efficiently is applied. This scheme involves relating the terms u_{xx} and u_{xxxx} with u at two adjacent nodal points to get a three-point implicit scheme. The Helmholtz equation [or Eq. (3)] is approximated as follows for $f_i = -(u_i^2 + \frac{1}{2} u_{x,i}^2 + 2\kappa u_i)$

$$\begin{aligned} &P_{i+1} - \left(2 + h^2 + \frac{1}{12} h^4 + \frac{1}{360} h^6\right) P_i + P_{i-1} \\ &\quad = h^2 f_i + \frac{1}{12} h^4 \left(f_i + \frac{\partial^2 f_i}{\partial x^2}\right) + \frac{1}{360} h^6 \left(f_i + \frac{\partial^2 f_i}{\partial x^2} + \frac{\partial^4 f_i}{\partial x^4}\right). \end{aligned} \tag{8}$$

The derived modified equation $\frac{\partial^2 P}{\partial x^2} - P = f + \frac{h^6}{20160} \frac{\partial^8 P}{\partial x^8} + \frac{h^8}{1814400} \frac{\partial^{10} P}{\partial x^{10}} + \cdots + H.O.T.$ for (3) shows that the proposed three-point compact difference scheme is indeed sixth-order accurate.

C. Symplectic Time Integration Scheme

The sixth-order accurate symplectic structure-preserving numerical integrator [34] is used to conserve symplecticity existing in the currently investigated nondissipative Hamiltonian system, leading to

$$u^{(1)} = u^n + \Delta t \left[\frac{5}{36} F^{(1)} + \left(\frac{2}{9} + \frac{2\tilde{c}}{3} \right) F^{(2)} + \left(\frac{5}{36} + \frac{\tilde{c}}{3} \right) F^{(3)} \right], \tag{9}$$

$$u^{(2)} = u^n + \Delta t \left[\left(\frac{5}{36} - \frac{5\tilde{c}}{12} \right) F^{(1)} + \left(\frac{2}{9} \right) F^{(2)} + \left(\frac{5}{36} + \frac{5\tilde{c}}{12} \right) F^{(3)} \right], \tag{10}$$

$$u^{(3)} = u^n + \Delta t \left[\left(\frac{5}{36} - \frac{\tilde{c}}{3} \right) F^{(1)} + \left(\frac{2}{9} - \frac{2\tilde{c}}{3} \right) F^{(2)} + \frac{5}{36} F^{(3)} \right], \tag{11}$$

$$u^{n+1} = u^n + \Delta t \left[\frac{5}{18} F^{(1)} + \frac{4}{9} F^{(2)} + \frac{5}{18} F^{(3)} \right]. \tag{12}$$

In the above, $\tilde{c} = \frac{1}{2}\sqrt{\frac{3}{5}}$ and $F^{(i)} = F(u^{(i)}, P^{(i)})$, $i = 1, 2, 3$. Calculation of the solution u^{n+1} from Eq. (12) needs to solve Eqs. (9)–(11) implicitly so as to get the values of $u^{(1)}$, $u^{(2)}$ and $u^{(3)}$ from the above symplectic Runge–Kutta scheme. The Helmholtz equation (3) is then solved to get $P^{(1)}$, $P^{(2)}$, and $P^{(3)}$. Upon reaching the specified convergence criteria, we can get first the solution u^{n+1} and then the solution P^{n+1}. The above iterative procedures are repeated until the difference, cast in a L_2-norm form, of the solutions calculated from two consecutive iterations falls below the user's specified tolerance (10^{-9} used in the current study).

D. Analysis and Verification of the Proposed Scheme

The equation $u_t + cu_x = 0$ will be used as the model for the verification and analysis of the proposed scheme given in Sections IV.A. The solution to this model equation is $u = \hat{u}_\alpha(t) e^{\mathbf{i}\alpha x}$, where $\mathbf{i} \equiv \sqrt{-1}$ and $\hat{u}_\alpha$ is the Fourier mode of the wavenumber α. Differentiation of the exact solution leads to $\frac{\partial u}{\partial x}|_{\text{exact}} = \mathbf{i}\alpha h \frac{\hat{u}_\alpha}{h} e^{\mathbf{i}\alpha x}$. Note that the wavenumber has been scaled by the gird spacing $h = \frac{L}{N}$, where L and N denote the length of physical domain and the number of grid intervals, respectively. This derivative term can be written as

$$\left. \frac{\partial u}{\partial x} \right|_{\text{numerical}} = \mathbf{i}\alpha' h \frac{\hat{u}_\alpha}{h} e^{\mathbf{i}\alpha x} = (K_\mathbf{r} + \mathbf{i} K_\mathbf{i}) \frac{\hat{u}_\alpha}{h} e^{\mathbf{i}\alpha x}. \tag{13}$$

In the above, $K_\mathbf{i} (= \Re[\alpha' h])$ and $K_\mathbf{r} (= -\Im[\alpha' h])$ accounting for the dispersion and dissipation errors are the real and imaginary parts of $\alpha' h$, respectively.

The computed values of $K_\mathbf{i}$ and $K_\mathbf{r}$ are plotted with respect to the scaled (or modified) wavenumber αh in Fig. 1. It can be easily seen that the proposed upwinding combined compact difference scheme performs better than the CCD scheme in [35, 36] owing to the improved dispersive accuracy while the positive-valued $K_\mathbf{r}$, on the contrary, is less accurate than the nondissipative (or $K_\mathbf{r} = 0$) centered-type combined compact difference scheme of Chu and Fan [36].

To verify the proposed scheme, the solution of the wave equation $u_t + 0.1u_x = 0$ will be sought subject to the initial condition given by $u(x, 0) = e^{-20000(x-x_0)^2} \cos[50(x - x_0)]$, where $x_0 = 7.998778998779$. Subject to the periodic boundary condition, the solution is sought at the time step chosen to be $\Delta t = \Delta x$ in 4096 uniformly distributed grids. Figure 2 shows the negligibly small computed difference between the exact waveform and the waveform obtained from the present scheme at $t = 30$.

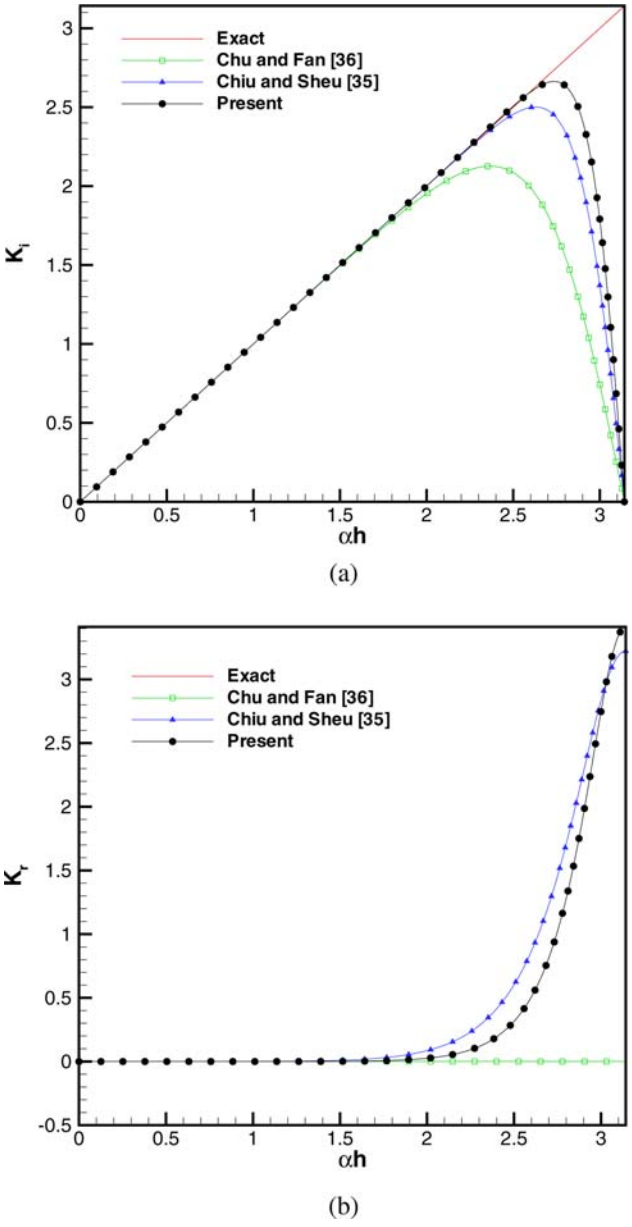

FIG. 1. Comparison of the profiles K_r and K_i with respect to the modified wavenumber αh amongst the proposed sixth-order accurate optimized upwinding combined compact difference scheme, fifth-order accurate upwinding combined compact difference scheme (CCD-5th) [35], and the three-point sixth-order accurate centered combined compact difference scheme (CCD-6th) [36]. (a) K_i; (b) K_r. [Color figure can be viewed in the online issue, which is available at wileyonlinelibrary.com.]

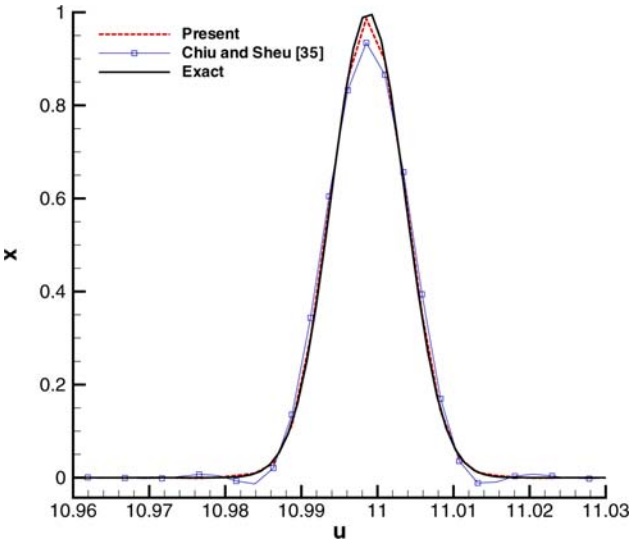

FIG. 2. Comparison of the present, Ref. [35],and exact solutions for the wave equation obtained at $t = 30$ in the domain of 4096 nodal points. [Color figure can be viewed in the online issue, which is available at wileyonlinelibrary.com.]

V. NUMERICAL RESULTS

The proposed scheme will be verified first by solving the CH equation at $\kappa = 0$ in Section V.A to get the peakon solution and at $\kappa > 0$ in Section V.II to get the peakon, cuspon and soliton solutions. The following Hamiltonians will be computed and plotted with respect to time for each test problem for indirectly verifying the proposed scheme based on the predicted CH solution

$$H_0 = \int u dx, \tag{14}$$

$$H_1 = \frac{1}{2}\int (u^2 + u_x^2) dx, \tag{15}$$

$$H_2 = \frac{1}{2}\int (u^3 + u u_x^2 + 2\kappa u^2) dx. \tag{16}$$

A. Numerical Studies of the CH Equation at $\kappa = 0$

Subject to smooth and nonsmooth initial conditions, whether these time-evolving solutions of (1) obtained at $\kappa = 0$ are classified to be the traveling type or are evolved to have different speeds and phase shifts will be examined.

Smooth Initial Condition

Traveling Wave Solution. In this example, the CH equation is solved at $\kappa = 0$. Given the initial conditions $\phi(0) = 1$ and $\phi_x(0) = 0$, the smooth traveling solution in a periodic domain has the solution form given by $u(x, t) = \phi(x - ct)$. Here, ϕ is the solution of the second-order ordinary

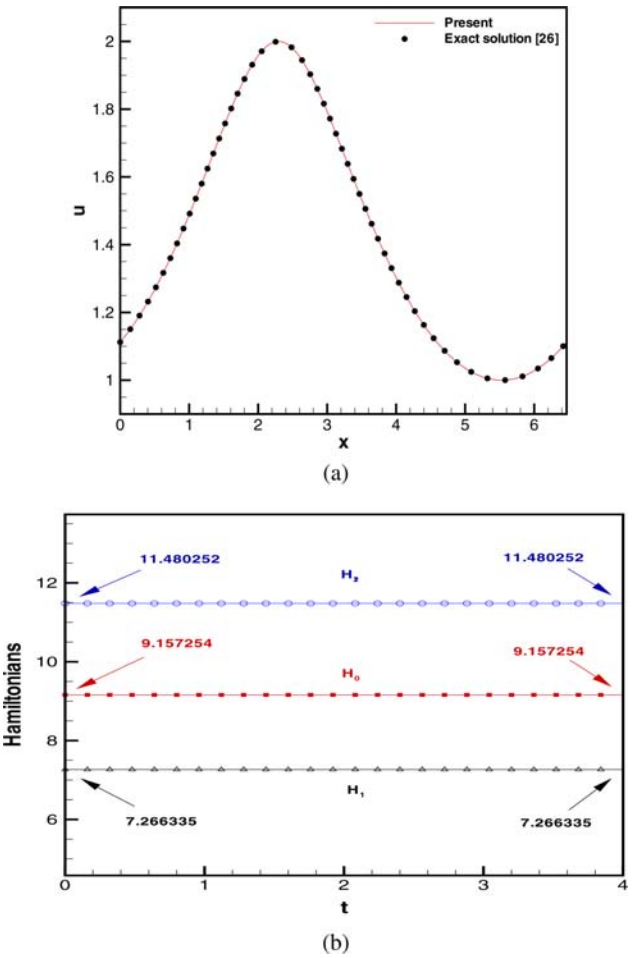

FIG. 3. (a) The smooth traveling wave solution predicted at $t = 4$ for the case of $\kappa = 0$ in a domain of 8192 grids; (b) The computed Hamiltonians H_0, H_1 and H_2 are plotted with respect to time. [Color figure can be viewed in the online issue, which is available at wileyonlinelibrary.com.]

differential equation $\phi_{xx} = \phi - \frac{\tilde{\alpha}}{(\phi - c)^2}$. Provided that $\tilde{\alpha} = c = 3$, the period of the resulting smooth traveling wave is approximately equal to 6.46954603635 [15, 26]. The predicted solution profile at $t = 4$, which is plotted in Fig. 3(a), agrees well with the exact solution. It can be clearly seen from Fig. 3(b) that the Hamiltonians H_0, H_1, and H_2 don't change their values all the time.

Nontraveling Wave Solution. The smooth initial condition $u_0 = \mathrm{sech}(x)$ is then considered in a periodic domain of length $L = 40$, which is uniformly divided into 8192 cells. Figure 4(a) shows the predicted solution at $t = 5.0$. The time step chosen for this calculation is $\Delta t = 0.05\Delta x$. The Hamiltonians H_0, H_1, and H_2 plotted in Fig. 4(b) are conserved very well.

Nonsmooth Initial Condition

Traveling Wave Solution. In $-20 \leq x \leq 20$, Eq. (1) is solved at $\kappa = 0$ to numerically demonstrate that CH equation permits the solitary wave solution (or peakon) given by the exact solution

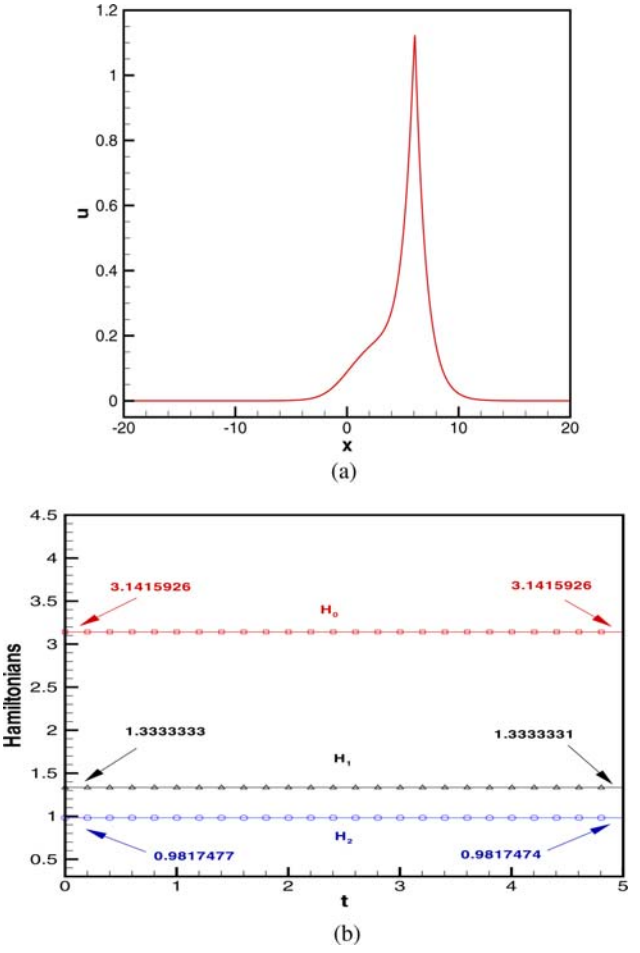

FIG. 4. (a) The non-traveling wave solution predicted at $t = 5$ for the case of $\kappa = 0$ in a domain of 8192 grids and (b) The predicted Hamiltonians H_0, H_1, and H_2 are plotted with respect to time. [Color figure can be viewed in the online issue, which is available at wileyonlinelibrary.com.]

$u(x,t) = ce^{-|x-ct|}$. This peaked solitary wave solution satisfies the CH equation everywhere except at the wave crest $x = c\,t$, where c denotes the phase speed. As a result, this close-form solution is known as the weak solution of (1) according to the work of Constantin and Molinet [37].

Given the initial solution $u(x,t=0) = e^{-|x|}$, the CH solution will be sought subject to the periodic boundary conditions prescribed at $x = \pm 20$ under $\Delta x = \frac{5}{514}$ and $\Delta t = 0.02\Delta x$. In Fig. 5(a), the peakon solution predicted in a domain of 4096 uniformly discretized grids is compared excellently with the exact result. As no wave breaking has been observed, this peakon problem is known to have a global traveling wave solution. Under our expectation, all the Hamiltonians shown in Fig. 5(b) remain unchanged with time.

Nontraveling Wave Solution. In this example, we consider the case with $u_0(x) = \frac{10}{(3+|x|)^2}$, which has a discontinuous derivative in $0 \le x,y \le 30$. In Fig. 6(a), the solution obtained in the domain

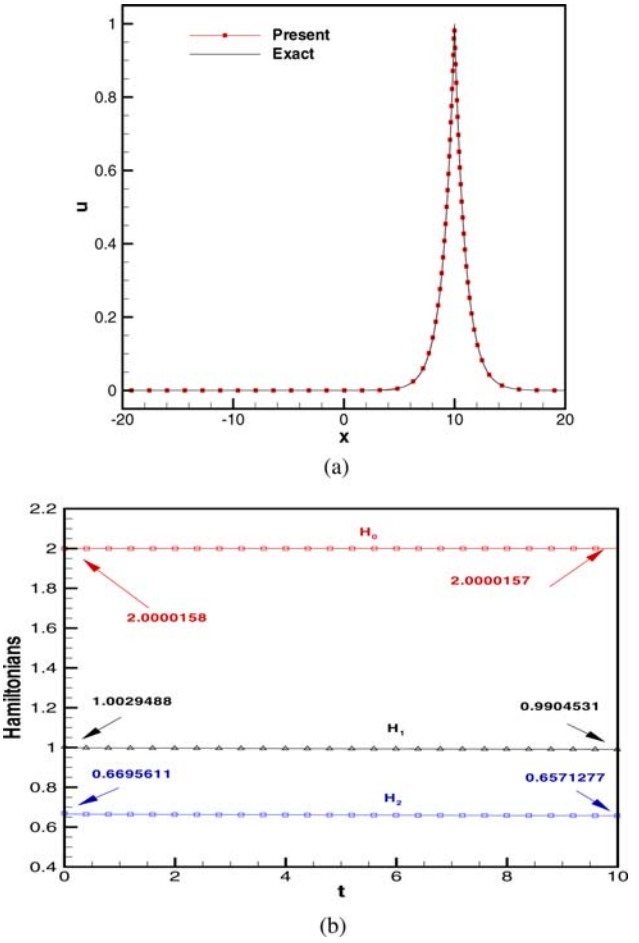

FIG. 5. (a) Comparison of the predicted and exact peakon solutions computed in a domain of 4096 grids at $t = 10$ and (b) The computed Hamiltonians H_0, H_1 and H_2 are plotted with respect to time. [Color figure can be viewed in the online issue, which is available at wileyonlinelibrary.com.]

of 8192 grids at $t = 20$ compares very well with the solutions in [26]. In Fig. 6(b), the quantities H_0, H_1, and H_2 are still conserved very well regardless of the predicted nontraveling wave solutions.

B. Numerical Studies of the CH Equation at $\kappa > 0$

More recently, the closed-form solutions of the peaked solitary wave type for the KdV, BBM (Benjamin–Bona–Mahony) and Boussinesq equations were derived in [38]. All the derived peaked solitary wave solutions satisfy their respective physically meaningful Rankine–Hogoniot jump conditions. They are therefore considered as the weak solutions of their corresponding shallow water equations. Another KdV-type shallow water equation was also shown to have the soliton, peakon, and cuspon solutions [39]. While these closed-form solutions have been derived under the traveling wave assumption and the wave-symmetry condition, none of these peaked solitary

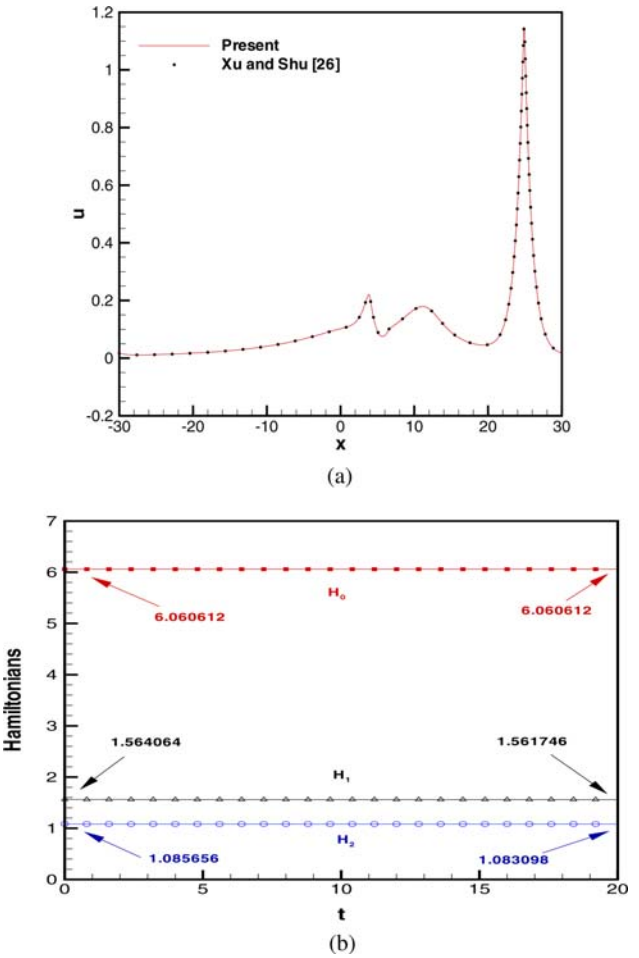

FIG. 6. (a) Comparison of the predicted and numerical solutions in a domain of 8192 grids at $t = 20$ and (b) The computed Hamiltonians H_0, H_1 and H_2 are plotted with respect to time. [Color figure can be viewed in the online issue, which is available at wileyonlinelibrary.com.]

waves have been observed numerically or experimentally. We are therefore motivated to clarify whether the CH equation permits traveling peaked solitary wave solution for $\kappa > 0$ in (1).

Initial Condition of Smooth Solitary Wave Type

Traveling Wave Solution. The following analytic problem admitting a periodic traveling wave solution $u(x,t) = U(x - ct)$ is chosen to solve the nonlinear CH equation at $\kappa > 0$ [17]

$$U' = \pm\sqrt{\frac{-U^3 + (c - 2\kappa)U^2 + C(A)\,U}{c - U}}. \tag{17}$$

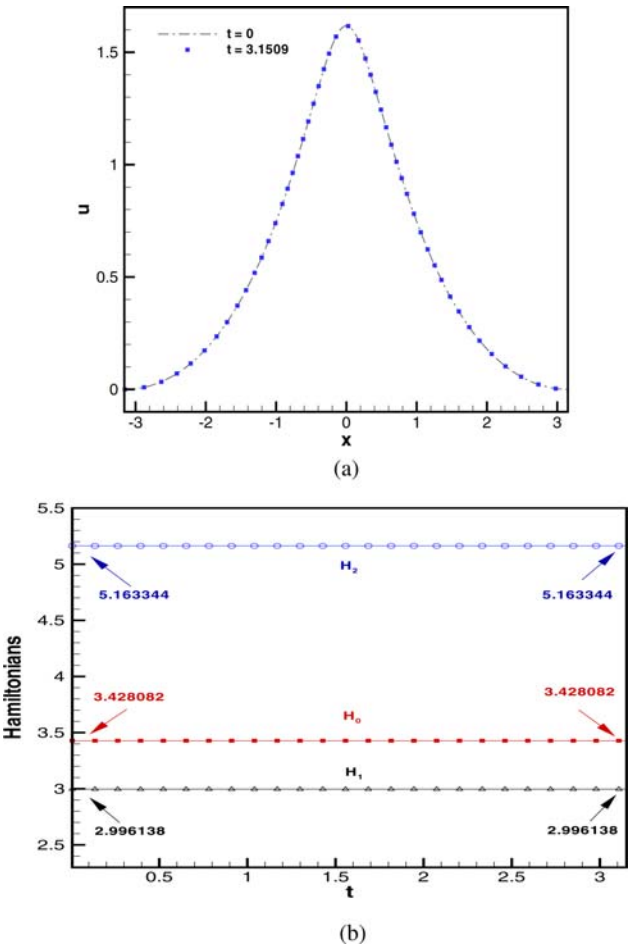

FIG. 7. (a) The predicted smooth traveling wave solutions at $\kappa = \frac{1}{2}$ in a domain of 256 grids at $t = 3.1509$ and (b) The computed Hamiltonians H_0, H_1, and H_2 are plotted with respect to time. [Color figure can be viewed in the online issue, which is available at wileyonlinelibrary.com.]

In the above, c and A are denoted as the wave speed and the wave amplitude, respectively. Integration of Eq. (17) leads to the expression

$$x = \frac{2}{\sqrt{a_1(a_2 - a_3)}}(a_1 - a_2)\Pi, \tag{18}$$

where Π is the elliptic function, $a_1 = c$, $a_2 = \frac{1}{2}(c - 2\kappa + \sqrt{(c - 2\kappa)^2 + 4C}$, and $a_3 = \frac{1}{2}(c - 2\kappa - \sqrt{(c - 2\kappa)^2 + 4C})$. Verification of the code will be carried out at $c = 2$, $\kappa = 1/2$, $C = 1$, $\Delta t = \frac{1}{4}\Delta x$ and $\Delta x = 0.0246166$. In Fig. 7(a), the predicted waveform matches excellently with its initial waveform. The values of H_0, H_1, and H_2 given in (14–16) are also calculated. It can be clearly seen from Fig. 7(b) that all the Hamiltonians don't change with time and remain to be equal to the initial values of 3.428082, 2.996138, and 5.163344 for H_0, H_1, and H_2, respectively. According to the results in Table I, the proposed method is sixth-order accurate and has the smallest L_2 norm error for the case solved in the finest mesh.

TABLE I. The predicted L_2-error norms at $t = 3.1509$ for the results obtained at $\Delta t = 0.00615415$ and different mesh spacings in $-3.15092964 \leq x \leq 3.15092964$.

Grid number	L_2 error norms	Rates of convergence
32	4.096896E-3	
64	3.702604E-5	6.78985
256	2.794334E-8	5.18591

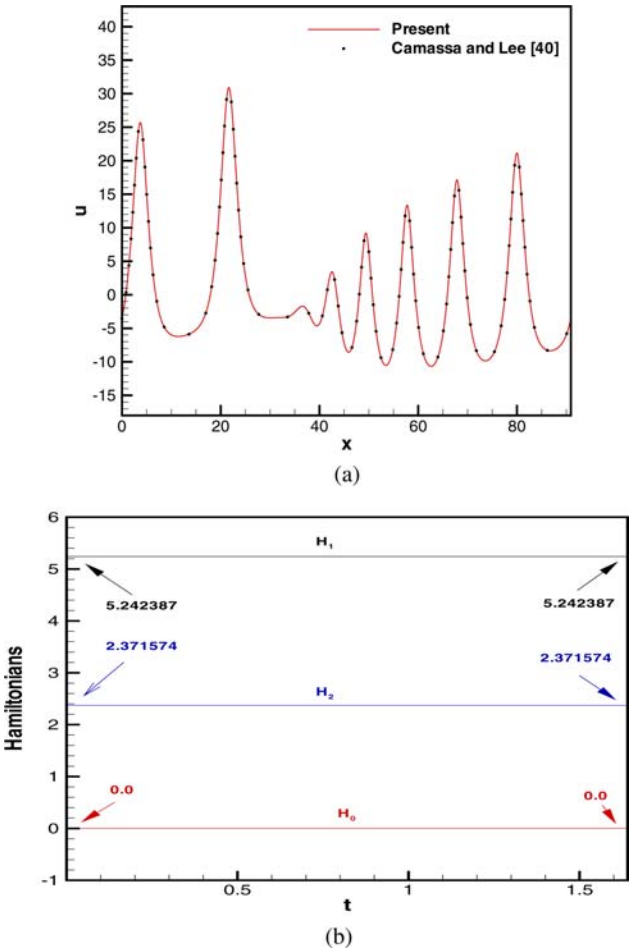

FIG. 8. (a) The predicted non-traveling wave solution for the case of $\kappa = \frac{1}{0.044}$ in a domain of 8192 grids at $t = 1.64$; (b) The computed Hamiltonians H_0, H_1, and H_2 are plotted with respect to time. [Color figure can be viewed in the online issue, which is available at wileyonlinelibrary.com.]

Nontraveling Wave Solution. According to Camassa and Lee [40], Eq. (1) will be solved at $\kappa = \frac{1}{2\delta}$ subject to the initial condition $u(x, 0) = \frac{1}{3\delta}\cos(\pi\delta x)$ and the periodic boundary condition $u(0, t) = u(\frac{2}{\delta}, t)$, where $\delta = 0.022$. This shallow-water wave tends to develop a discontinuity [29]. We choose this problem to demonstrate the ability of applying the proposed scheme to resolve sharp solution.

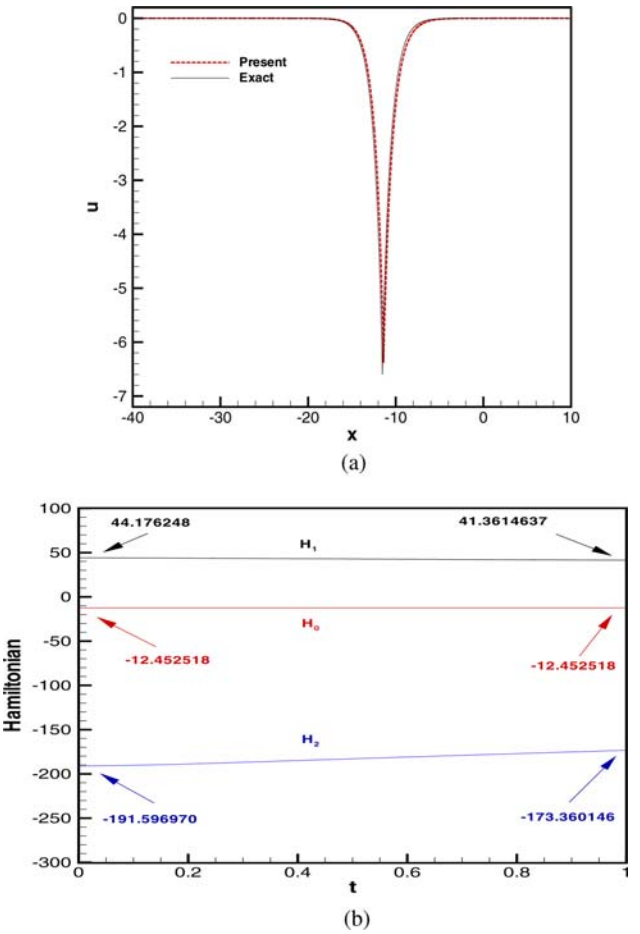

FIG. 9. (a) The predicted cuspon traveling wave solutions at $\kappa = \frac{1}{10}$ in a domain of 32768 grids at t = 1.0; (b) The computed Hamiltonians H_0, H_1, and H_2 are plotted with respect to time. [Color figure can be viewed in the online issue, which is available at wileyonlinelibrary.com.]

In the domain of the length $\frac{2}{0.022}$ or 90.91, the solutions of the CH equation will be solved in the uniformly distributed 8192 nodal points. One can see from Fig. 8(a) that the nonoscillatory solution predicted in this study compares fairly well with the particle solution. Similar to all the examples studied in the previous sections, the computed values of H_0, H_1, and H_2 in Fig. 8(b) show that the proposed numerical method indeed can preserve all the theoretically conserved quantities. Note that in Fig. 8(b) the values of H_1 and H_2 have been divided by 1000 and 100,000, respectively.

Initial Condition of Nonsmooth Solitary Wave Type

Traveling Wave Solution. We solve the problem with the cuspon solution given below [28]

$$u(y,t) = \frac{2p^2cv}{(c^2+p^2)-(c^2-p^2)\cosh\xi}, \quad x = 2cy + \ln\left(\frac{g}{h}\right). \tag{19}$$

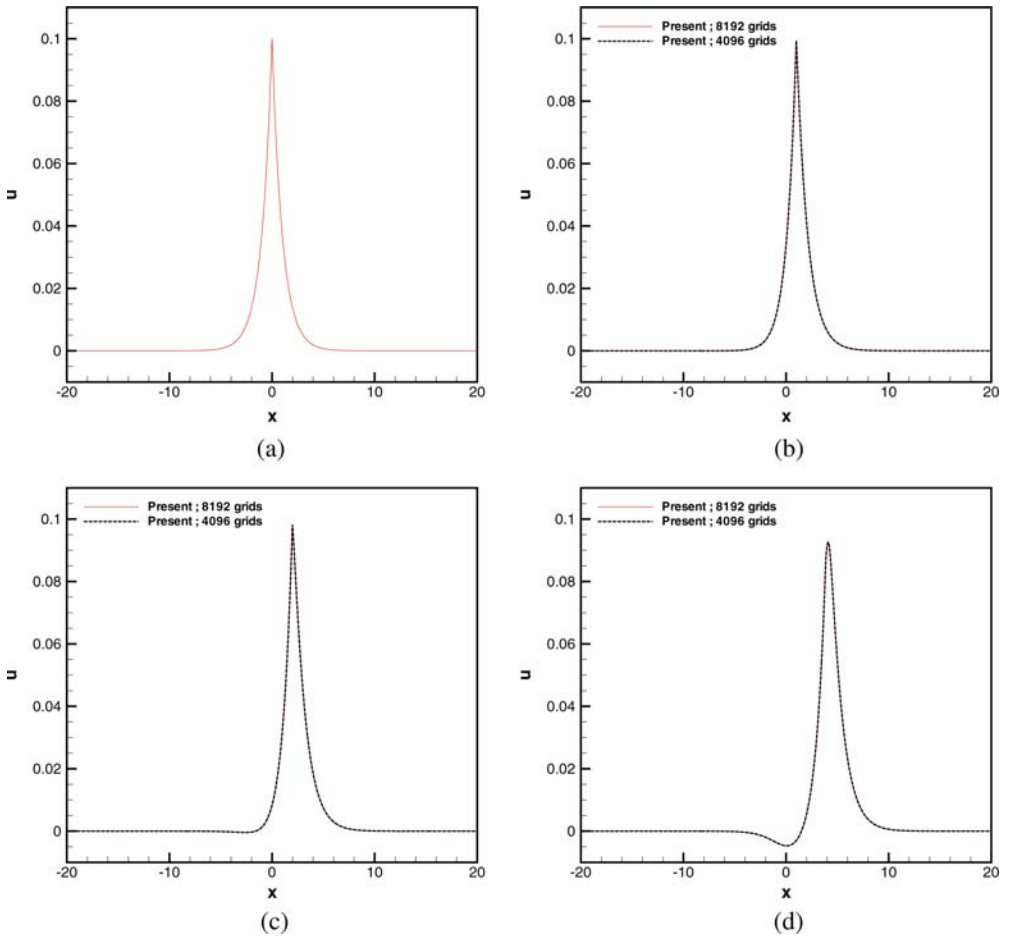

FIG. 10. The predicted non-traveling peakon solutions at $\kappa = \frac{1}{100}$ in a domain of 4096 and 8192 grids at different times. (a) $t = 0$; (b) $t = 10$; (c) $t = 20$; and (d) $t = 40$. [Color figure can be viewed in the online issue, which is available at wileyonlinelibrary.com.]

In the above, $g = 1 - (\frac{c-p}{c+p})e^{\xi}$, $h = 1 - (\frac{c+p}{c-p})e^{\xi}$, $\xi = p(2y - vt)$, $v = \frac{2}{c^2-p^2}$ with $c = \frac{1}{\kappa} = 10.0$ and $p = 10.15$. The time-evolving cuspon solution was predicted in $-2.0 \leq y \leq 1.5$ containing 32768 uniformly discretized grids. Figure 9(a) shows good agreement between the results that are plotted at $t = 1.0$. For the verification sake, we also plot in Fig. 9(b) the values of H_0 and H_1, which are all unchanged with time except H_2, for the case investigated at $\kappa = 0.1$.

Through the study of this problem, we found that the peaked solitary wave solution can remain orbitally stable. A wave initially close to a peaked solitary wave type can remain approximately the same for all times. This computational finding agrees with the stability analysis in [8].

Nontraveling Wave Solution. The truncated solution of the fifth-order HAM solution [9] is considered as the initial condition given below

$$u_0(x) = 0.10010204081632653061224489795 9e^{-\frac{7|x|}{5\sqrt{2}}} - 0.00010204081632653061 22e^{-\frac{7\sqrt{2}|x|}{5}}. \quad (20)$$

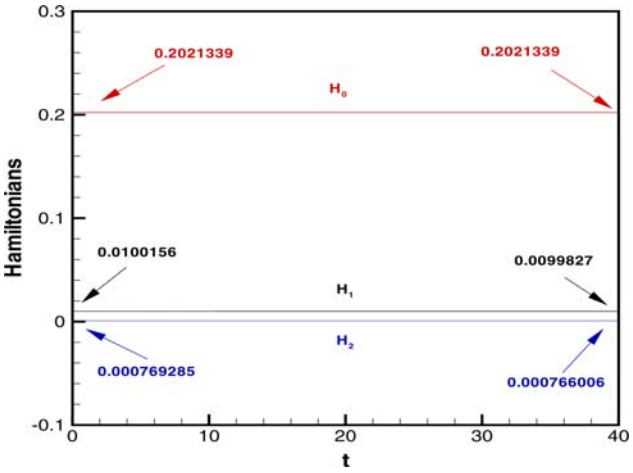

FIG. 11. The predicted Hamiltonians H_0, H_1 and H_2 are plotted with respect to time for the problem of nontraveling wave peakon given in Section "nontraveling wave solution." [Color figure can be viewed in the online issue, which is available at wileyonlinelibrary.com.]

TABLE II. The conclusion drawn from the cases carried out on the CH equation at $\kappa = 0$ and $\kappa > 0$. The notation "——" means that no solution is available for making the validation or the verification study.

Problem	κ	Initial solution	Wave nature	H_0, H_1 and H_2	status
5.1.1.1	0	$u_{xx} = u - \frac{3}{(u-3)^2}$	Traveling	Conserved	Verified
5.1.1.2	0	$u_0(x) = \mathrm{sech}(x)$	Nontraveling	Conserved	——
5.1.2.1	0	$u_0(x) = e^{-\lvert x\rvert}$	Traveling	Conserved	Verified
5.1.2.2	0	$u_0(x) = \frac{10}{(3+\lvert x\rvert)^2}$	Nontraveling	Conserved	Validated
5.2.1.1	>0	Eq.(17)	Traveling	Conserved	Verified
5.2.1.2	>0	$u_0(x) = \frac{1}{3\delta}\cos(\pi\delta x)$	Nontraveling	Conserved	Validated
5.2.2.1	>0	Eq. (19)	Traveling	Conserved	Verified
5.2.2.2	>0	Eq. (20)	Nontraveling	Conserved	——

Note that this initial solution is the perturbed HAM solution derived in [9]. The grid refinement study is performed first. The solutions are computed at two different numbers of cells $N = 4096$ and $N = 8192$ in the domain of $-20 \leq x \leq 20$. In Fig. 10, the peakon at $t = 0$ was found to suddenly change to its shape and then gradually becomes smooth. The predicted results enlighten that the prescribed perturbation has led to another wave with different speeds and phase shifts. As a result, the stability of solitary wave needs to be analyzed in terms of the orbital stability by examining if this wave can remain close to some translate of the starting solitary wave at later times. In other words, whether or not the shape of the wave remains approximately the same for all times needs to be further clarified in the future study. The values of H_0, H_1, and H_2 plotted in Fig. 11 are all unchanged with time for the case investigated at $\kappa = 0.01$.

Based on the solution of (1) predicted at $\kappa > 0$ by using the proposed symplecticity-preserving and numerical modified wavenumber optimized scheme, the conclusion drawn from this series of studies of the CH equation at $\kappa = 0$ and $\kappa > 0$ is summarized in Table II. Depending on the perturbation added to the simulation, the peaked solitary wave solution for (1) at $\kappa > 0$ can remain to be orbitally stable all the time or, on the contrary, can be evolved to become a new one with different

speeds and phase shifts. In other words, our conclusion agrees with Constantin and Strauss [8] and Camassa et al. [7], respectively.

VI. CONCLUDING REMARKS

To reduce the differential order, the CH equation has been transformed to a set of equations governing respectively the transport of solution variables u and P. In this $u - P$ formulation, following the method of lines the time derivative term is approximated by the sixth-order accurate implicit symplectic Runge–Kutta scheme to preserve Hamiltonians. As for the first-order spatial derivative terms, the numerical wavenumber error predicted from the proposed sixth-order accurate upwinding combined compact difference scheme has been minimized. Another emphasis of this study is to clarify that the CH equation with/without inclusion of the linear first-order advection term admits the traveling and nontraveling wave solutions for the problems subject to the initial solutions taking the smooth soliton, solitary peakon, and cuspon forms. In short, our study computationally supports the finding of Camassa, Holm and Hyman (1994) who concluded that peaked solitary wave is amenable to the CH equation at $\kappa = 0$. On the contrary, this study also supports the conclusion of Constantion and Strauss (2002) who pointed out that peaked solitary wave solution can be orbitally stable provided that $\kappa > 0$. In other words, the CH solution can remain approximately the same as its initial peaked solitary wave for all times.

References

1. A. B. De Monvel, A. Kostenko, D. Shepelsky, and G. Teschl, Long-time asymptotics for the Camassa-Holm equation, SIAM J Math Anal 41 (2009), 1559–1588.
2. D. D. Holm and M. F. Staley, Wave structure and nonlinear balances in a family of evolutionary PDEs, SIAM J Appl Dyn Syst 2 (2003), 323–380.
3. A. Degasperis and M. Procesi, Asymptotic integrability, A. Degasperis and G. Gaeta, editors, Symmetry and perturbation theory, World Scientific Publishing, 1999, pp. 23–27.
4. Tony W. H. Sheu, P. H. Chiu, and C. H. Yu, On the development of a high-order compact scheme for exhibiting the switching and dissipative solution natures in the Camassa-Holm equation, J Comput Phys 230 (2011), 5399–5416.
5. H. Holden and X. Raynaud, Global conservative solutions of the Camassa-Holm equation-a Lagrangian point of view, Comm Partial Diff Equat 32 (2006), 1511–154.
6. D. Cohen, B. Owren, and X. Raynaud, Multi-symplectic integration of the Camassa-Holm equation, J Comput Phys 227 (2008), 5492–5512.
7. R. Camassa, D. Holm, and J. Hyman, A new integrable shallow water equation, Adv Appl Mech 31 (1994), 1–33.
8. A. Constantin and W. A. Strauss, Stability of Camassa-Holm solitons, J Nonlinear Sci 12 (2002), 415–422.
9. S. J. Liao, Homotopy analysis method in nonlinear differential equations, Springer & Higher Education Press, Heidelberg, 2012.
10. R. Camassa and D. Holm, An integrable shallow water equation with peaked solitons, Phys Rev Lett 71 (1993), 1661–1664.
11. T. J. Bridges and S. Reich, Multi-symplectic integrators: numerical schemes for Hamiltonian PDEs that conserve symplecticity, Phys Letter A 284 (2001), 184–193.

12. M. Stanislavova and A. Stefanov, On global finite energy solutions of the Camassa-Holm equation, J Fourier Anal Appl 11 (2005), 511–531.

13. S. Hakkaev, Stability of peakons for an integrable shallow water equation, Phys Letter A 354 (2006), 137–144.

14. J. Lenells, Stability of periodic peakons, Int Math Res Notices 10 (2004), 485–499.

15. P. H. Chiu, L. Lee, and T. W. H. Sheu, A dispersion-relation-preserving algorithm for a nonlinear shallow-water wave equation, J Comput Phys 228 (2009), 8034–8052.

16. P. H. Chiu, L. Lee, and T. W. H. Sheu, A sixth-order dual preserving algorithm for the Camassa-Holm equation, J Comput Appl Math 233 (2010), 2267–2278.

17. R. Camassa and L. Lee, A complete integral particle method for a nonlinear shallow-water wave equation in periodic domains, DCDIS, Series A 14 (2007), 1–5.

18. R. Camassa, Characteristics and initial value problem of a completely integrable shallow water equation, Discrete Continuous Dyn Syst Ser B 3 (2003), 115–139.

19. R. Camassa, J. Huang, and L. Lee, On a completely integral numerical solution for a nonlinear shallow-water wave equation, J Nonlinear Math Phys 12 (2005), 146–162.

20. R. Camassa, J. Huang, and L. Lee, Integral and integrable algorithm for a nonlinear shallow-water wave equation, J Comput Phys 216 (2006), 547-572.

21. H. Holden and X. Raynaud, A convergent numerical scheme for the Camassa-Holm equation based on multipeakons, Discrete Contin Dyn Syst 14 (2006), 503–523.

22. H. Holden and X. Raynaud, Convergence of a finite difference scheme for the Camassa-Holm equation, SIAM J Numer Anal 44 (2006), 1655–1680.

23. H. Kalisch and J. Lenells, Numerical study of traveling-wave solutions for the Camassa-Holm equation, Chaos, Solitons Fractals 25 (2005), 287–298.

24. H. Kalisch and X. Raynaud, Convergence of a spectral projection of the Camassa-Holm equation, Numer Method Part D E 22 (2006), 1197–1215.

25. R. Artebrant and H. J. Schroll, Numerical simulation of Camassa-Holm peakons by adaptive upwinding, Appl Numer Math 56 (2006), 695–711.

26. Y. Xu and C. W. Shu, A local discontinuous Galerkin method for the Camassa-Holm equation, SIAM J Numer Anal 46 (2008), 1998–2021.

27. T. Matsuo and H. Yamaguchi, An energy-conserving Galerkin scheme for a class of nonlinear dispersive equations, J Comput Phys 228 (2009), 4346–4358.

28. B. -F. Feng, K. Maruno and Y. Ohta, A self-adaptive mesh method for the Camassa-Holm equation, J Comput Appl Math 235 (2010), 229–243.

29. Y. Ohta, K -I. Maruno and B. -F. Feng, An integrable semi-discretization of the Camassa-Holm equation and its determinant solution, J Phys A: Math Theor 41 (2008), 355205.

30. R. I. McLachlan, Symplectic integration of Hamiltonian wave equations, Numer Math 66 (1994), 465–492.

31. T. J. Bridges and S. Reich, Numerical methods for Hamiltonian PDEs, J Physics A 39 (2006), 5287–5320.

32. C. K. W. Tam and J. C. Webb, Dispersion-relation-preserving finite difference schemes for computational acoustics, J Comput Phys 107 (1993), 262–281.

33. G. Ashcroft and X. Zhang, Optimized prefactored compact schemes, J Comput Phys 190 (2003), 459–477.

34. W. Oevel and M. Sofroniou, Symplectic Runge-Kutta schemes II: classification of symmetric method, University of Paderborn, Germany, Preprint, 1997.

35. P. H. Chiu and T. W. H. Sheu, On the development of a dispersion-relation-preserving dual-compact upwind scheme for convection-diffusion equation, J Comput Phys 228 (2009), 3640–3655.

36. P. C. Chu and C. Fan, A three-point combined compact difference scheme, J Comput Phys 140 (1998), 370–399.

37. A. Constantin and L. Molinet, Global weak solutions for a shallow water equation, Commun Math Phys 211 (2000), 45–61.

38. S. J. Liao, Two kinds of peaked solitary waves of the KdV, BBM and Boussinesq equations, Sci China, Phys, Mechan Astron 55 (2012), 2469–2475.

39. A. M. Wazwaz, A modified KdV-equaiton that admits a variety of travelling wave solutions: kinks, solitons, peakons and cuspons, Phys Scr 86 (2012), 045501.

40. R. Camassa and L. Lee, Complete integrable particle methods and the recurrence of initial states for a nonlinear shallow-water wave equation, J Comput Phys 227 (2008), 7206–7221.